remote sensing

MDPI

Article

Improvement of Workflow for Topographic Surveys in Long Highwalls of Open Pit Mines with an Unmanned Aerial Vehicle and Structure from Motion

Ignacio Zapico [1,2,*], Jonathan B. Laronne [3], Lázaro Sánchez Castillo [4] and José F. Martín Duque [1,2]

[1] Geodynamics, Stratigraphy and Paleontology Department, Complutense University, 28040 Madrid, Spain; josefco@ucm.es
[2] Instituto de Geociencias, IGEO (CSIC, UCM), 28040 Madrid, Spain
[3] Department of Geography and Environmental Development, Ben-Gurion University of the Negev, P.O. Box 653, Beer-Sheva 84105, Israel; john@bgu.ac.il
[4] Department of Mining and Geologic Engineering, Polytechnic University of Madrid, 28003 Madrid, Spain; lazaro.sanchez@upm.es
* Correspondence: izapico@ucm.es

Abstract: Conducting topographic surveys in active mines is challenging due ongoing operations and hazards, particularly in highwalls subject to constant and active mass movements (rock and earth falls, slides and flows). These vertical and long surfaces are the core of most mines, as the mineral feeding mining production originates there. They often lack easy and safe access paths. This framework highlights the importance of accomplishing non-contact high-accuracy and detailed topographies to detect instabilities prior to their occurrence. We have conducted drone flights in search of the best settings in terms of altitude mode and camera angle, to produce digital representation of topographies using Structure from Motion. Identification of discontinuities was evaluated, as they are a reliable indicator of potential failure areas. Natural shapes were used as control/check points and were surveyed using a robotic total station with a coaxial camera. The study was conducted in an active kaolin mine near the Alto Tajo Natural Park of East-Central Spain. Here the 140 m highwall is formed by layers of limestone, marls and sands. We demonstrate that for this vertical landscape, a facade drone flight mode combined with a nadir camera angle, and automatically programmed with a computer-based mission planning software, provides the most accurate and detailed topographies, in the shortest time and with increased flight safety. Contrary to previous reports, adding oblique images does not improve accuracy for this configuration. Moreover, neither extra sets of images nor an expert pilot are required. These topographies allowed the detection of 93.5% more discontinuities than the Above Mean Sea Level surveys, the common approach used in mining areas. Our findings improve the present SfM-UAV survey workflows in long highwalls. The versatile topographies are useful for the management and stabilization of highwalls during phases of operation, as well closure-reclamation.

Keywords: highwall; mining; topography; SfM-UAV; accuracy

Citation: Zapico, I.; Laronne, J.B.; Sánchez Castillo, L.; Martín Duque, J.F. Improvement of Workflow for Topographic Surveys in Long Highwalls of Open Pit Mines with an Unmanned Aerial Vehicle and Structure from Motion. *Remote Sens.* **2021**, *13*, 3353. https://doi.org/10.3390/rs13173353

Academic Editor: Amin Beiranvand Pour

Received: 26 July 2021
Accepted: 21 August 2021
Published: 24 August 2021

1. Introduction

Open-pit mining activities substantially modify the land, creating new landscapes associated with excavated (open pit areas) and accumulated (waste dump) landforms, which are prone to experience geomorphic hazardous processes such as mass movements (falls, slides or flows), erosion, or subsidence [1]. These threats are predominantly monitored and controlled using topographic studies based on detailed High Resolution Topographies [2]. These data sources are a requirement for the correct design of mine closure plans [3]. Among the topographic instruments/methods available to survey mining areas, the most common is the combination of Structure from Motion (SfM) photogrammetry and the use of Unmanned Aerial Vehicles (SfM-UAV), as detailed elsewhere [4]. In complex topographic

areas, such as mining areas, some SfM-UAV studies [5] have reported higher point cloud densities and accuracy than traditional methods such as Terrestrial Laser Scanning (TLS). They are also produced at the lowest cost and reduce field work. The SfM-UAV technique is presently accepted as a standard procedure for engineering geology applications [6]. Several choices are involved when conducting such surveys. Three of the most important are: flight drone mode, camera angle, and method of georeferencing.

SfM-UAV surveys have a fast, flexible and easy-to-use workflow that usually implies automatic deployment of a drone flight at a constant altitude Above Mean Sea Level (AMSL), imaging in nadir mode to ensure desired overlap, and scaling as well as georeferencing the final topography with control points measured in the field [7]. This standard procedure has been successfully used in a wide range of environments such as landslides [8], rivers [9] and agricultural areas [10]. However, in zones with steep slope gradients, keeping a constant altitude Above Ground Level (AGL) is almost mandatory to obtain a constant Ground Sampling Distance (GSD). Maintaining a constant AMSL altitude with the aim to obtain a specific GSD value is not possible in a landscape with high relief, because those topographic changes imply changes in the final GSD of images taken, ranging from few (1.7–2.9) centimeters [11] to several (2–7) centimeters [12]; these may affect future stability analyses based on these topographies. AMSL surveys are commonly used in geomorphic studies of mining areas [13]. Improving the final accuracy can be achieved by following three different strategies: (i) a combination of several missions at different altitudes; (ii) conducting manual flights and changing the altitude with a camera time-lapse function [14]; or, (iii) using a specific computer-based mission planning software, which allows the user to program the drone to automatically keep a constant AGL, thereby the drone continuously varies its flight altitude to adapt to changes in relief [15]. The latter is an example of how this type of software becomes operational in steep terrains. Recently, facade flight modes have been used in earth science studies [16]. Primarily designed for surveying buildings, these allow users to program a drone to conduct vertical flights, and can be used in other landscapes such as cliffs and highwalls.

Camera angle is an important issue in the use of SfM-UAV surveys conducted in high relief landscapes. It is widely accepted that SfM processing based on oblique images (off-nadir) in addition to nadir improves the final topography, reducing the final error by as much as half [5] and preventing systematic errors due to doming [17]. Indeed, SfM-UAV surveys processed with images taken from different angles enable more detailed topographies to be obtained in areas with intricate geometry or sudden changes in slope [18]. Several angle options have been proposed. For instance, it is suggested that images be taken at 13–35° tilt angles in addition to nadir ones to improve precision, although these can reduce the final accuracy [11]. Other suggested angles are 0–10° [12], 20–40° [19] and 45° [15]. Flights with a dynamic camera angle focused on a Point of Interest may produce the smallest systematic errors [20].

Another major issue to consider in SfM-UAV surveys of high relief landscapes is the manner by which control and check points are deployed and measured. This is the most demanding task in vertical or quasi-vertical surfaces, such as mining highwalls. In very steep topographies, such as cliffs, the most common strategy is to allocate points at the top or bottom and measure them with a differential GPS [12,19] and/or a total station [21]. This is somewhat impractical in many mining highwalls, because no access exists to the top or bottom areas. Moreover, the terrain may be dangerous. In other cases, a TLS is also simultaneously used to obtain a reference point cloud from which points are extracted [22]. Although this is an effective solution, it is expensive and time consuming, losing most of the advantages of running SfM-UAV surveys. A cheaper georeferencing method is to extract control points from public aerial photogrammetric flight mission data. This procedure has been tested in part of the Ihlara Valley in the Cappadocia Region, where a vertical landscape was surveyed using smartphone images with promising results [23]. However, two main disadvantages exist: (i) the difficulty to find common points between two sets of images surveyed at a significant difference in time, and with different resolution;

(ii) the reference topography can only provide points at the bottom or upper parts of the valley. These factors reduce the quality of the final results and, depending on the surveyed landscape, the quality may be insufficient for undertaking some analyses. Under these conditions, the only method by which to obtain reliable control/check points is to search for highlighted points such as corners, artifacts or pedestrian crossing lines, and measure their coordinates with a total station with the reflectorless option [6,24].

Recent SfM-UAV studies in mining areas have been mainly focused on multi-temporal surveys to detect general geomorphic changes [25], or specific erosive features such as gullies [13,26]. Others have focused on the automatic delimitation of features in active areas, such as mining banks [2]. Despite the increase in the use of SfM-UAV topographies in the monitoring of mined areas, several challenges remain, such as how to survey long mining highwalls to obtain sufficient detail and accuracy to identify cracks or discontinuities. These allow early risk detection of future slope instabilities such as rockfalls, frozen soil falls, and debris flows.

Highwalls are complex and demanding in terms of conducting a topographic survey, since they usually incorporate high vertical relief with no proper and safe access to either their crest or base. Digital terrestrial photogrammetry is being successfully carried out in the walls of mines to detect discontinuities [27], however its action range is limited to short distances, with UAVs required to survey long highwalls [28,29]. The authors of [30] studied the slope stability of a highwall with UAV images taken at 100 m above ground, and [31] conducted another survey with images acquired at 50 m to map geological units. These two examples were carried out at a constant AMSL altitude and did not face the challenge of vertically surveying a highwall with the objective to obtain more detailed topographies. In [32], a 33 m height highwall was surveyed with centimeter accuracy by adding vertically-acquired drone images. The authors georeferenced the survey with control points placed around the wall. Similarly, [33] carried out some SfM-UAV surveys in vertical 50–60 m height walls of quarries; however, as a novelty they measured control-check points directly on the wall with a total station, demonstrating how topographies derived from such procedure can be successfully used to identify discontinuities in rock mass zones. In [28], a vertical survey was conducted of a 100 m-heigh marble highwall, and the accurate identification of discontinuities were reported. The drone was manually driven, requiring an expert pilot to overcome the risks that face such a vertical shape. The point cloud was georeferenced with points from a reflectorless total station.

Several attempts have been made to design safe, cheap, simple, and flexible acquisition of SfM-UAV procedures in highwalls, with few studying discontinuity characterization. The novelty of our study lies in our attempt to conduct such topographic surveys with a computer-based mission planning software in long highwalls (>100 m) of active kaolin mines, a complex landscape that is as yet unreported with regard to SfM-UAV survey procedures. We evaluate several drone flight settings and camera angles, focusing on the extent to which facade drone flight mode images can independently produce such high accurate and detailed topographies. We also tackle georeferencing the surveys in such a landscape. Our objective is to simplify and improve previous SfM-UAV workflows based on data obtained in extreme vertical terrain.

2. Materials and Methods

2.1. Study Area

The Spanish kaolin production is mainly developed in the Iberian System. Within this area, two large mines, Machorro and Maria José (Figure 1) are located in the surroundings of the Alto Tajo Natural Park [34]. This landscape has high erosion potential, due to the existence of loose sandy and clayed mine wastes, steep and long slopes, and high rainfall erosivity. Here, local authorities limit mining activity to companies applying the best available technologies and environmental practices. In this erosive context, these two active mines are currently applying some of those practices: fluvial geomorphic reclamation [3], and the maintenance of sedimentation pond systems with automatic hydrological and

sedimentary monitoring stations [35]. Two other abandoned mines are responsible for environmental problems: landslides [5] and sediment-related water pollution [36].

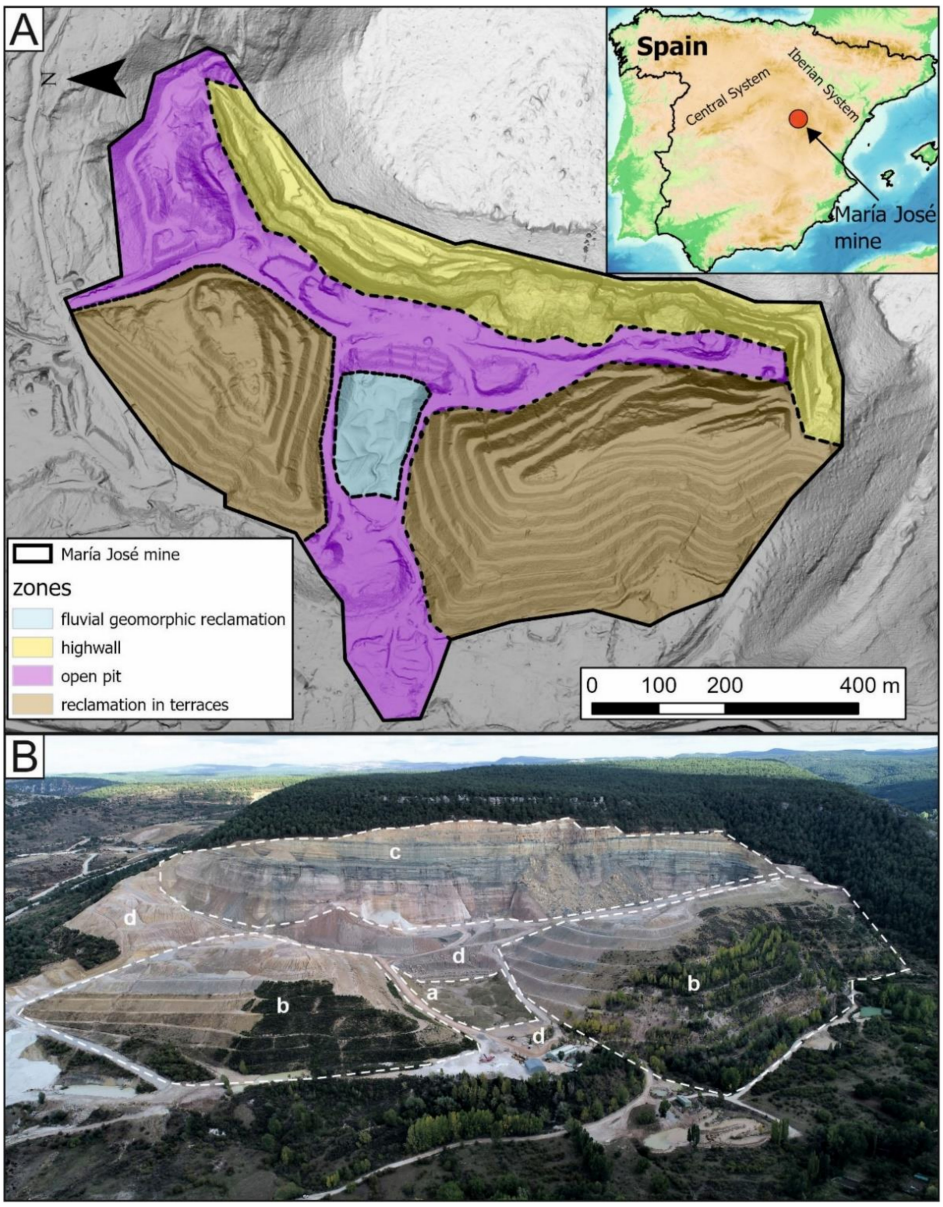

Figure 1. Location and map (**A**), and oblique view of the María José mine on 15 April 2018 (**B**). The mine is classified into four areas: (a) a fluvial geomorphic-based reclamation; (b) two terraced waste dumps; (c) a highwall; (d) an open pit with ponds, roads and other work areas. Base topography in (**A**) derived from a LiDAR point cloud provided by the Spanish National Plan for Aerial Orthophotography of 2018; photo by DGDRONE (2020).

The active Maria José mine includes the following areas (Figure 1): a 140-m highwall subject to differential weathering, with overhanging, fractured and jointed rock complexities along steep slopes; an open pit with sedimentation ponds; two large terraced waste dumps; and a fluvial geomorphic-based reclamation. The highwall is formed by a unit of limestones and dolostones, marls, and kaolin sands, and is capped by a thin layer of topsoil (Figure 2). The exposed zones are usually stable; the owners perform continuous qualitative monitoring based on images and videos to identify possible risks, such as active cracks. Although here we use the concept of "long and vertical highwalls", for example higher than 100 m, in reality they are not entirely vertical. They include

safety berms, therefore forming a benched (berm-outslope) topography system (like a steep staircase), fulfilling the requirements of the so-called Complementary Technical Instructions (Chapter VII of the General Regulation of Basic Rules of Mining Safety; https://www.boe.es/buscar/doc.php?id=BOE-A-1990-9859, accessed on 20 July 2021).

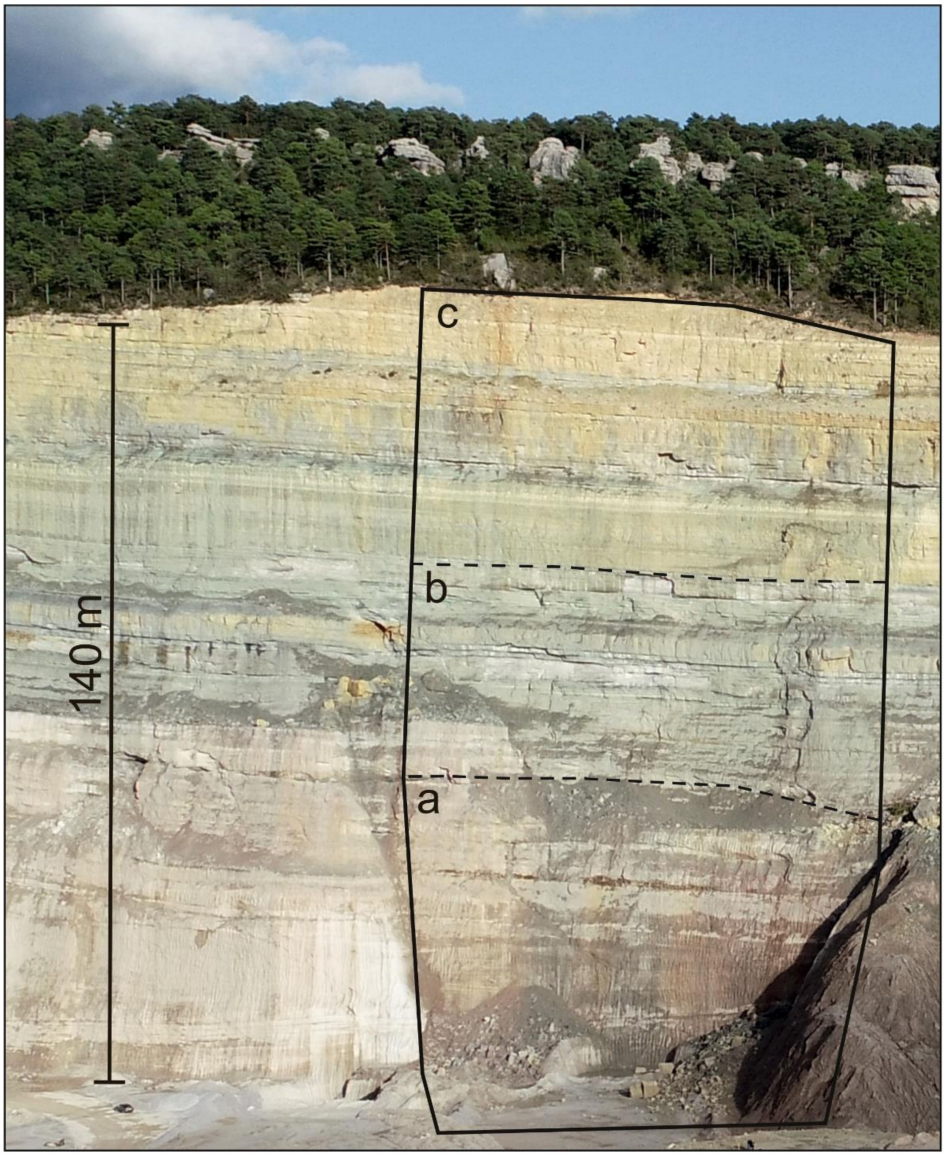

Figure 2. Oblique view of the studied sector in the highwall of the María José mine. (a) kaolin sands; (b) marls; (c) limestones and dolostones. Photo by DGDRONE (2020).

2.2. UAV Flight Planning and Surveying

Seven flight missions were conducted based on two parameters (Table 1 and Figure 3): (i) drone altitude mode and (ii) imaging angle. The flights were programed with the computer-based mission planning software UgCS [37]. This software has already been successfully used in a high-relief landscape [16] but not for a vertical landscape. It allows a detailed process flight plan based on a user-defined digital terrain model with a specified spatial image resolution. In addition to the two common altitude mode options, AGL or AMSL, this software also allows the drone to be programmed to follow a vertical trajectory with a specific overlap and GSD. Although this "facade scan" mode was initially designed for buildings, it can be applied to any flat or curved vertical surface, such as a mining highwall. Using either of the altitude modes, this software allows separate tilting of the camera between 0° and 90°. It also has a Point of Interest option, that changes the camera

position to continuously shoot toward a specific area. For this study we chose an angle of 40° for oblique pictures, because its final accuracy has been reported to increase in coastal cliffs [19]. Here the nadir angle occurs when the camera viewing direction is perpendicular to the entire surface (AGL and AMSL modes) or to the highwall (facade mode). The base topographies used as reference in the UgCS software were provided by the Spanish National Plan for Aerial Orthophotography of 2018 and by the company that runs the mine.

Table 1. Features of the seven conducted flight missions.

Flight Mission	A	B	C	D	E	F	G
flight speed (m s^{-1})	2	2	3	3	3	2	2
flight duration (min)	29	29	17	17	16	21	25
GSD (cm)	5	5	1.6	1.6	2.2	1.1	1.1
forward/side overlap (%)	75	75	75	75	75	75	75
camera angle (°)	nadir	40 off-n	nadir	40 off-n	POI	nadir	40 off-n
flight type	AMSL	AMSL	AGL	AGL	AGL	facade	facade
double grid (Y/N)	Y	Y	Y	Y	Y	Y	Y
number of images	384	380	154	163	97	125	136

POI (Point of Interest); AMSL (Above Mean Sea Level); AGL (Above Ground Level); off-nadir (off-n).

All the flights were conducted on 25 September 2020 by a DJI Phanton 4 Pro drone with a similar forward/side overlap of 75% and double grid pattern. We chose this setting combination, instead of the common 80–60% overlap and single grid, since the double grid ensures a high overlap without taking redundant images. Flight velocity (2–3 m s^{-1}) and duration (16–29 min) varied. Flight operation required one or two batteries for each mission.

2.3. Georeferencing and Data Accuracy: Field Survey

Altogether, 34 points were surveyed with the Leica M60 MultiStation for use as control (georeferencing) or check points (accuracy assessment). This instrument has a robotic coaxial camera that allows the user to identify points at a millimeter scale up to a distance of 1 km. Since it was not possible to access the highwall crest (no available paths) nor the bottom (rockfall hazard) areas, characteristic natural features such as rock corners, fissures or color changes were used. These were surveyed with the aim to homogeneously cover the entire highwall, and to efficiently identify them in the images.

The MS60 also has a laser scan function, which was used to survey the same study area. In some aspects, using a TLS can be disadvantageous with respect to an SfM-UAV procedure, however, it is considered a reliable instrument to check image-based topographies [18], since it has fewer error sources. Based on this assumption, a point cloud was surveyed during the same field campaign to identify systematic errors in the SfM-UAV topographies. The highwall was scanned from two positions. As the MS60 was georeferenced in the field using six points measured with a Leica differential 1200 GPS, both scans and total station points were directly georeferenced and no further reregistration or processing was required. The accuracy of the scanned point cloud was calculated with five cross-painted marks placed far from highwall risk zones; these were measured with the total station.

2.4. Data Processing

Images from each flight mission were loaded and processed as separated chunks (data sets) in the SfM software Agisoft Metashape Professional edition, version 1.6.5.11249 [38]. The alignment step was conducted with the following parameterization: Accuracy—Highest; Generic preselection—on; key point limit—200,000; Tie point limit—0; Adaptative camera model fitting—on; camera self-calibration. Each spare point cloud was filtered using the Gradual Selection tools termed 'Reconstruction Uncertainty' and 'Projection Accuracy'. Control/check points were thereafter added to each chunk, their number varying among surveys because some could not be identified in the images. A minimum of 15 control points was used to process

each survey as suggested elsewhere [39]; the rest were used as check points. Where the number of control/check points was smaller than 15, all were used as control points. A final Gradual Selection tool 'Reprojection error' was applied following suggested tips and steps [40]. Dense point clouds were obtained following the next parametrization: Quality—Ultra High; Depth filtering—Aggressive; Calculate point color and confidence—on. The 'Point confidence' feature, which allows the user to remove outliers, arose during the densification process. Other obtained products were raster files such as Digital Elevation Models (DEMs) and orthophotos. Although two types of DEMs exist—surface and terrain, we do not distinguish between them here, since the studied highwall section did not have vegetation nor other non-ground features. Agisoft software was run in a Dell Precision Tower 3620 with a processor Intel Core i7-6700 (4CPUs), a memory RAM of 65GB, a graphic card NVIDIA Quadro K2200, and a 500 GB SSD hard disk.

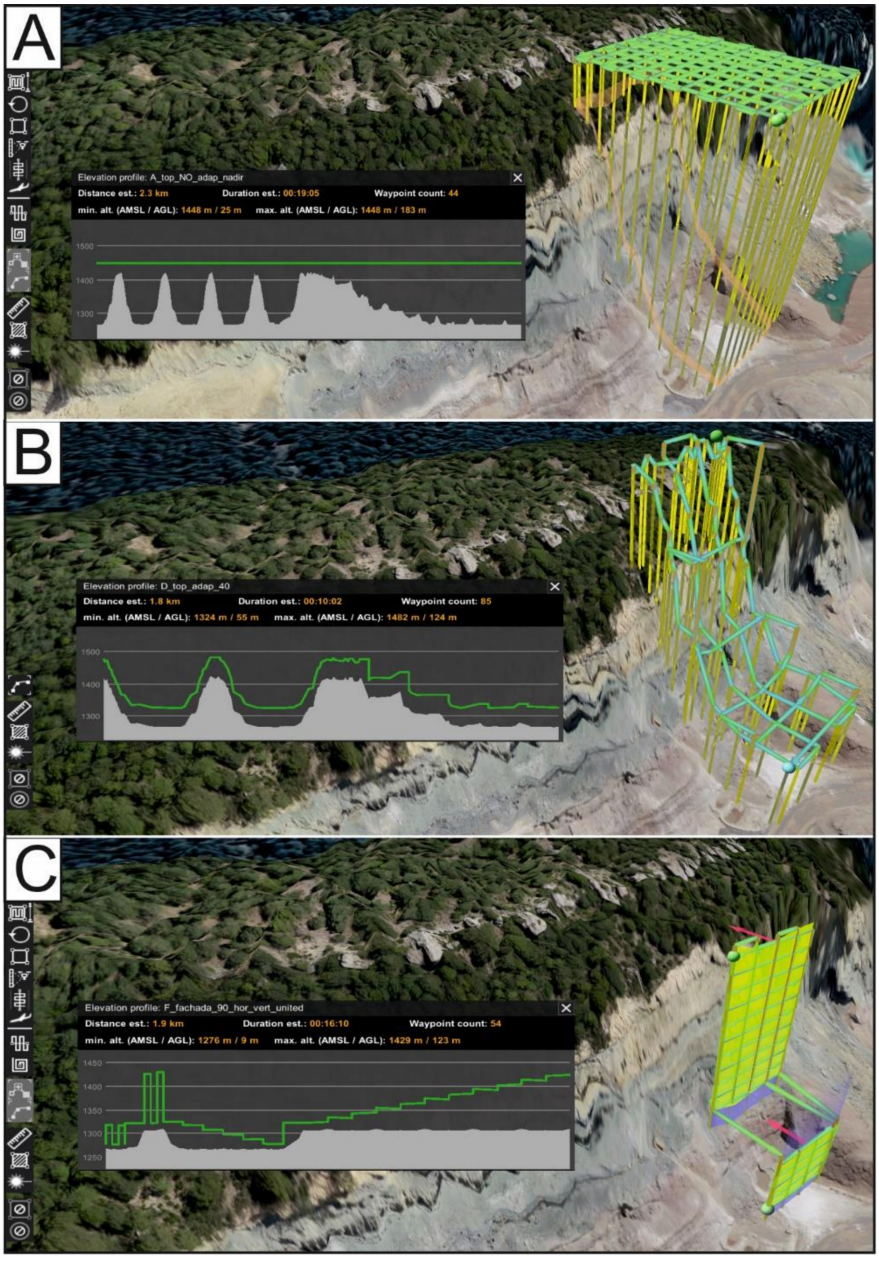

Figure 3. View of the flight missions and profiles programmed with the computer-based mission planning software UgCS: Above mean sea level, nadir and 40° off-nadir angles (**A**); Above ground level, nadir, 40° off-nadir and Point of Interest angles (**B**); and facade, nadir and 40° off-nadir angles (**C**).

2.5. Quality Evaluation

Reliability has to be determined because SfM-UAV topographic surveys have a wide range of error sources, necessitating a clear identification of systematic errors and precision in the final results [41]. The residuals of the control points used to scale and to georeference each point cloud determine the registration error. The residuals of the check points define how a final topography represents reality. The mean absolute error (MAE) and the root-mean-square error (RMSE) of the residuals offer data accuracy, while the standard deviation determines the precision. These were used to identify the difference between multiple flight modes and camera angle settings. Systematic errors are low when the RMSE or the MAE are similar to the standard deviation.

The point cloud surveyed with the laser scan as a reference was analyzed to identify systematic errors associated with a poor distribution of the control points in some SfM-UAV surveys. Each SfM-UAV point cloud was loaded in the CloudCompare software [42] and compared to the TLS data set using the M3C2 distance algorithm tool. This calculates the distance between two-point clouds [43]. A statistical analysis based on a Pearson correlation was also conducted using the features of the surveys, as well as their registration errors, accuracies, and precision.

2.6. Detection of Discontinuities

To evaluate how discontinuities can be detected, a semiautomatic algorithm was run on selected point clouds located in limestones and dolostones (Figure 2). The Discontinuity Set Extractor software was used, since it is open-source, easy to use and has been previously employed on outcrops [44]. Using a dense point cloud as input, it allows a quick recognition of the main discontinuities, orientations and their associated number of clusters [45]. This semi-automatic software is run in three steps. Each of these defines statistical parameters/steps (figures in brackets): (i) location of local curvature, a nearest neighbor search to define the normal vectors, it defines the discontinuity orientation at every point (k-nearest neighbor—30; tolerance—0.2); (ii) a statistical analysis of the planes, it determines the main orientations of the discontinuities through a Kernel density estimation algorithm (number of bins—64; minimum angle—30°; maximum number of planes: 4; cone filter—30°); and (iii) a cluster analysis grouping the points that define each discontinuity in the space (k sigmas—1.5; fix normal vector—selected). The parameters used were those recommended by the authors.

3. Results

3.1. Point Cloud and Derived Product Features

A dense point cloud was obtained for each survey (Table 2; Figure 4); the final topographies differ in relation to the type of flight mission. Since all the topographies were processed using the same settings in Agisoft-Metashape software, the differences occur due to variations in both flight altitude mode and camera angle. Three flight missions produced point clouds covering almost the entire surveyed area: AMSL-nadir (A), AMSL-40° off-nadir (B) and facade-nadir (F). The other point clouds covered 75–80% of the area, having significant point voids on the highwall top, facade-40° off-nadir (G) generating an empty area in the middle. The number and distribution of control/check points also varied between point clouds. Two flight missions acquired adequate good quality images to identify the reference points over the entire surface: AMSL-40° off-nadir (B) and facade-nadir (F).

Table 2. Features of the processed SfM-UAV topographies listed in Table 1.

Mission/Survey ID:		A	B	C	D	E	F	G	F + G
Feature	**Unit**								
number of check points	#	0	10	2	4	10	2	0	4
number of control points	#	14	15	15	15	15	15	12	15
homogeneously distributed over the area	Y/N	N	Y	N	N	N	Y	N	Y
time alignment	h	2.6	2.7	0.8	3.1	0.5	0.6	0.75	4
time dense point cloud	h	77	22	21.5	16	10.5	3	9	17.5
reconstructed surface *	%	98	99	80	75	80	100	80	100
number of tie points	#	579,498	394,643	445,145	368,581	283,159	603,550	529,182	848,913
dense point cloud density	pts cm^{-2}	0.09	0.13	0.29	0.26	0.16	1.53	1.4	1.44
DEM resolution	cm	3.3	2.8	1.9	2.0	2.5	0.8	0.9	0.8

* refers to the proportion of reconstructed surface.

The most time-consuming task in the field (ca. 4 h) was surveying the 34 control/check points with the total station. Although the flight time for each survey was relatively short (17–29 min; Table 1), the computer processing time based on Agisoft reports widely varied, as the slow AMSL-nadir survey (A) consumed 100 h, while the fastest, the facade-nadir (F), took 3.6 h. In all cases the dense point cloud SfM step was the slowest, while the alignment action was the fastest.

In terms of point cloud density, only the facade surveys (F, G) were able to produce values greater than 1-point cm^{-2}, while the others varied in the range 0.09–0.29-point cm^{-2}. As expected, this point cloud density is notable in derived products such as DEMs (Figure 5) and orthophotos (Figure 6). AMSL and facade surveys were able to produce DEMs covering the entire survey area, however the facade provided more details. The only flight survey able to produce a detailed orthophoto of the highwall was the facade-nadir survey (F).

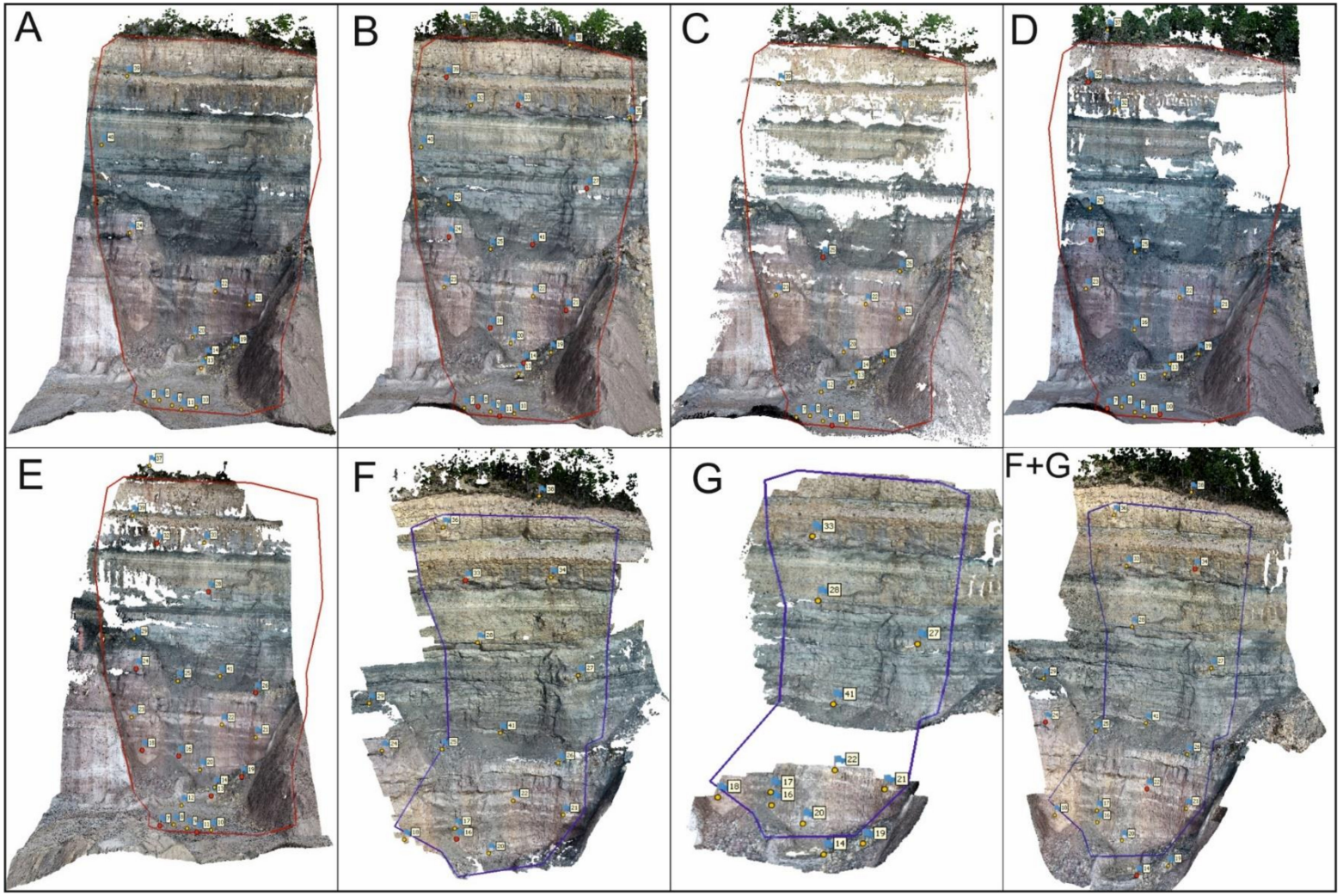

Figure 4. Dense point clouds showing the distribution of control (yellow) and check (red) points of the different SfM-UAV surveys. (**A**) AMSL-nadir; (**B**) AMSL-40° off-nadir; (**C**) AGL-nadir; (**D**) AGL-40° off-nadir, (**E**) AGL-Point of Interest; (**F**) facade-nadir; (**G**) facade-40° off-nadir.

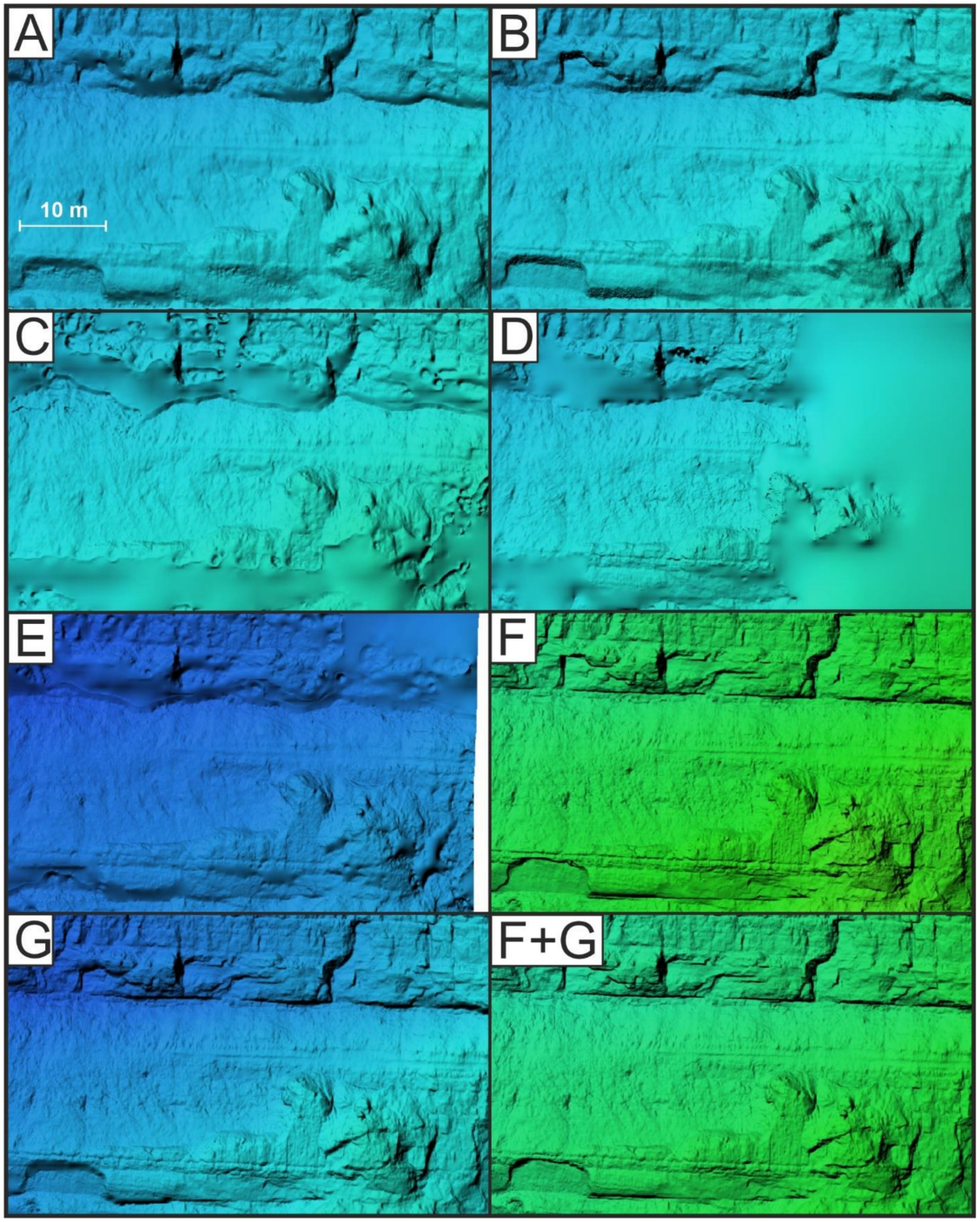

Figure 5. Details of the Digital Elevation Models obtained from the different SfM-UAV surveys. (**A**) AMSL-nadir; (**B**) AMSL-40° off-nadir; (**C**) AGL-nadir; (**D**) AGL-40° off-nadir, (**E**) AGL-Point of Interest; (**F**) facade-nadir; (**G**) facade-40° off-nadir.

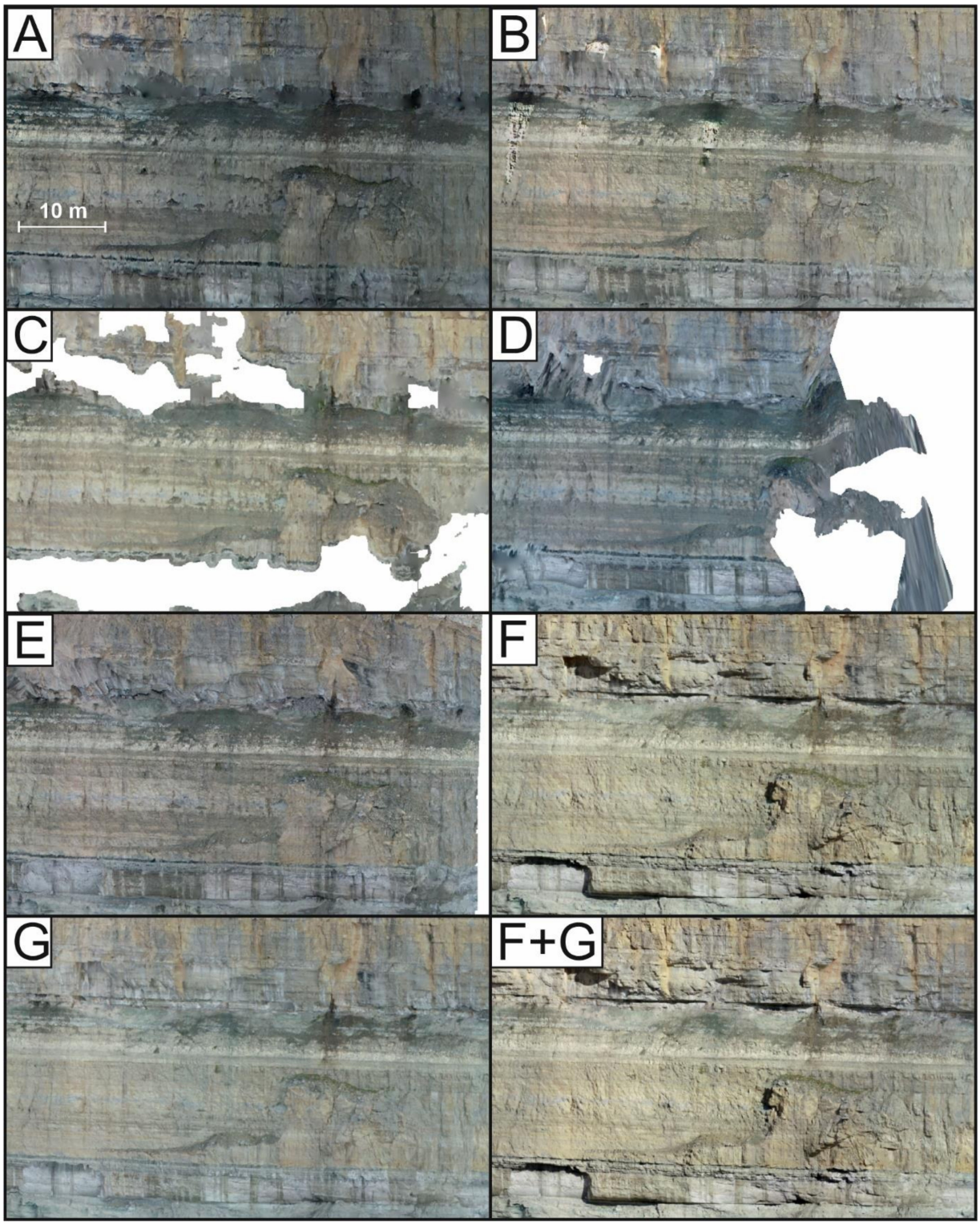

Figure 6. Details of the Orthophotos obtained from the different SfM-UAV surveys. (**A**) AMSL-nadir; (**B**) AMSL-40° off-nadir; (**C**) AGL-nadir; (**D**) AGL-40° off-nadir; (**E**) AGL-Point of Interest; (**F**) facade-nadir; (**G**) facade-40° off-nadir.

3.2. Quality Assessment of Point Clouds

The registration errors, accuracies and precisions of the various SfM reconstructions differed between the flight missions (Table 3). AMSL surveys (A, B) reported the highest registration errors, accuracy and precision figures, whereas the corresponding facade (F, G) quantities were the lowest.

Table 3. Data quality (cm) of the processed SfM-UAV topographies (see Table 1).

Parameter	A	B	C	D	E	F	G	F + G
n check points	0	10	2	4	10	2	0	4
				Registration of Control Points				
MAE x	3.8	3.8	3.2	1.8	4.7	1.4	1.5	1.2
MAE y	4.2	3.6	2.6	2.6	2.2	1.5	1.4	1.8
MAE z	6.7	5.2	3.8	3.3	3.7	1.0	1.6	1.1
MAE all	9.7	8.2	6.3	5.1	7.4	2.7	3.0	2.8
RMSE x	5.4	3.8	4.6	2.5	7.3	2.2	2.1	1.4
RMSE y	6.3	3.6	2.8	3.2	3.0	2.2	1.9	2.5
RMSE z	9.4	5.2	5.6	4.7	4.5	1.5	1.9	1.3
RMSE all	12.6	7.8	7.8	6.2	9.1	3.5	3.4	3.1
				Accuracy of Check Points				
MAE x	n/a	5.6	3.7	2.6	4.6	1.9	n/a	2.5
MAE y	n/a	2.5	5.1	1.0	2.9	0.9	n/a	0.5
MAE z	n/a	5.3	4.0	2.7	2.7	0.3	n/a	1.3
MAE all	n/a	9.2	7.8	4.1	6.6	2.2	n/a	3.0
RMSE x	n/a	10.3	3.8	3.3	5.4	2.4	n/a	3.0
RMSE y	n/a	3.6	5.5	1.2	3.9	1.1	n/a	0.5
RMSE z	n/a	6.5	5.5	3.1	3.6	0.3	n/a	1.4
RMSE all	n/a	11.8	8.6	4.7	7.6	2.7	n/a	3.4
				Final Precision				
SD x	n/a	9.3	5.2	2.4	5.4	2.8	n/a	2.8
SD y	n/a	3.4	2.9	1.3	3.2	0.9	n/a	0.6
SD z	n/a	6.8	5.6	2.0	3.4	0.2	n/a	1.6
SD all	n/a	7.8	5.2	2.7	4.0	2.3	n/a	1.7

'n/a'—check points not available.

For AMSL and AGL surveys the registration errors decreased when a 40° off-nadir camera angle was used. Conversely, the facade mode reduced registration error by using the nadir camera angle (F), rather than being set at the 40° off-nadir (G). Specifically, the reduction was larger than three quarters when compared with the errors reported by the most common drone configuration: AMSL with nadir images (A). The dynamic camera angle obtained with the Point of Interest configuration (E) also produced higher registration errors. The lowest registration error was obtained with the facade altitude mode combined with a nadir camera angle (F).

The registration trends also occurred for accuracy and precision, however, we cannot analyze the influence of camera angle in AMSL and facade flight modes in detail, because some surveys did not have check points. An AGL survey improved at 40° off-nadir. The lowest accuracy and lowest precision were obtained with the facade altitude mode combined with a nadir camera angle (F). In this case, accuracy and precision were almost equal when MAE was used, whereas the RMSE accuracy was lower than precision. From the Pearson correlation test between drone flight features and data quality results, we observed a positive (>0.7) correlation between GSD and 3D registration error, precision and accuracy, suggesting that the smallest GSD offer better quality results.

Since some of the SfM-derived reconstructions showed incomplete detection of the surveyed area and lacked homogeneous control/check point identification, a second data quality evaluation was run using the TLS point cloud as reference. This point cloud omitted areas of interest owing to relief shadows. Moreover, high wind speed affected the stability of the scanning on the right boundary, creating some vertical areas without points. Avoiding dangerous areas with rock and earth falls, six points deployed in the highwall base were used to evaluate TLS point cloud quality in terms of accuracy with RMSE (x—3.4 cm; y—4.7 cm; z—2.8 cm; all—6.6 cm), mean absolute error (x—2 cm; y—2.1 cm; z—2.6 cm; all—4.8 cm), and precision (x—3 cm; y—4.4 cm; z—2 cm; all—4 cm). The standard

deviation (precision) from these TLS-based cloud-to-cloud comparisons (Table 4) show how they correspond to those reported by the check points (r^2—0.97).

Table 4. Comparison of the final 3D precision (cm) for each SfM-UAV survey (A–G) obtained from two different independent reference data resources (check points and TLS). The number of points used in each comparison is stated in brackets.

Survey	Check Points	TLS
A	n/a (0)	6.4 (276,703)
B	7.8 (10)	5.5 (276,703)
C	5.2 (2)	4.6 (190,941)
D	2.7 (4)	3.1 (276,703)
E	4.0 (10)	3.7 (276,703)
F	2.3 (2)	2.5 (274,265)
G	n/a (0)	4.9 (276,703)
F + G	1.7 (4)	2.5 (276,703)

'n/a'—check points not available.

The comparisons are only considered for those zones where the points of both surveys are present. Altogether, the comparison exhibits a positive deviation, however it varies widely depending on the flight survey settings (Figure 7). Almost all of the error comparisons lacked a normal distribution, but were concentrated in some areas, occurring in point clouds of surveys with poor control point distribution (A, C, D, E and G). The facade-nadir angle flight configuration (F) produced an almost normal distribution of the error.

An extra dense point cloud was processed using images from both facade surveys with the aim to explore the resultant accuracy. Although this produced the highest number of tie points, the final point cloud was very similar to the one obtained by the facade-nadir mission (F) in terms of point cloud density, coverage area, control-check point distribution, quality of derived products, precision, and accuracy. Self-evidently, processing was more time-consuming.

3.3. Extraction of Discontinuities

The Discontinuity Set Extractor software was run on two point clouds (Table 5): AMSL mode with 40° off-nadir images (B), and facade mode with nadir pictures (F). These were the only outputs capable of producing point clouds without significant voids and with the highest accuracies and point cloud densities. The facade topography detected a larger number of main orientations and more clusters than the AMSL topography. The main difference was between the number of identified clusters: 2175 for F and 142 for B; i.e., 93.5 % more clusters. Figure 8 shows a comparison of discontinuities, where each colour represents the orientation of the main discontinuities.

Table 5. Comparison of the discontinuity orientations and clusters detected in two topographies using the Discontinuity Set Extractor software.

Flight Setting	AMSL with 40° Off-Nadir Pictures				Facade with Nadir Pictures				
n° of dip dir	1	2	3	4	1	2	3	4	5
dip dir (°)	278	106	234	209	285	296	135	223	262
dip (°)	49	88	68	86	50	86	4	78	90
n° of clusters	61	19	57	5	518	478	386	378	415

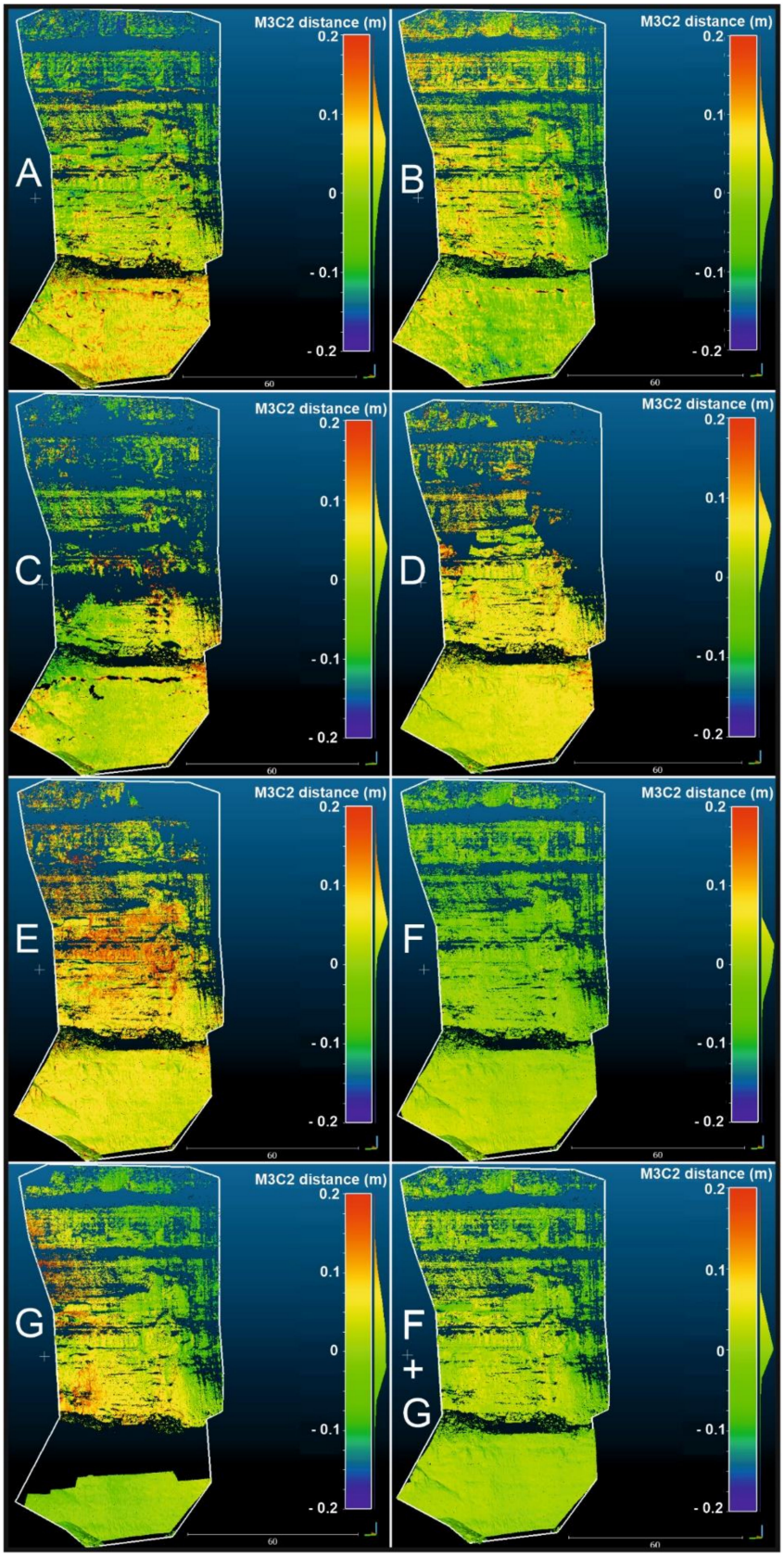

Figure 7. Comparison of data quality with the TLS algorithm of Cloud Compare by using the TLS point cloud as reference. (**A**) AMSL-nadir; (**B**) AMSL-40° off-nadir; (**C**) AGL-nadir; (**D**) AGL-40° off-nadir, (**E**) AGL-Point of Interest; (**F**) facade-nadir; (**G**) facade-40° off-nadir.

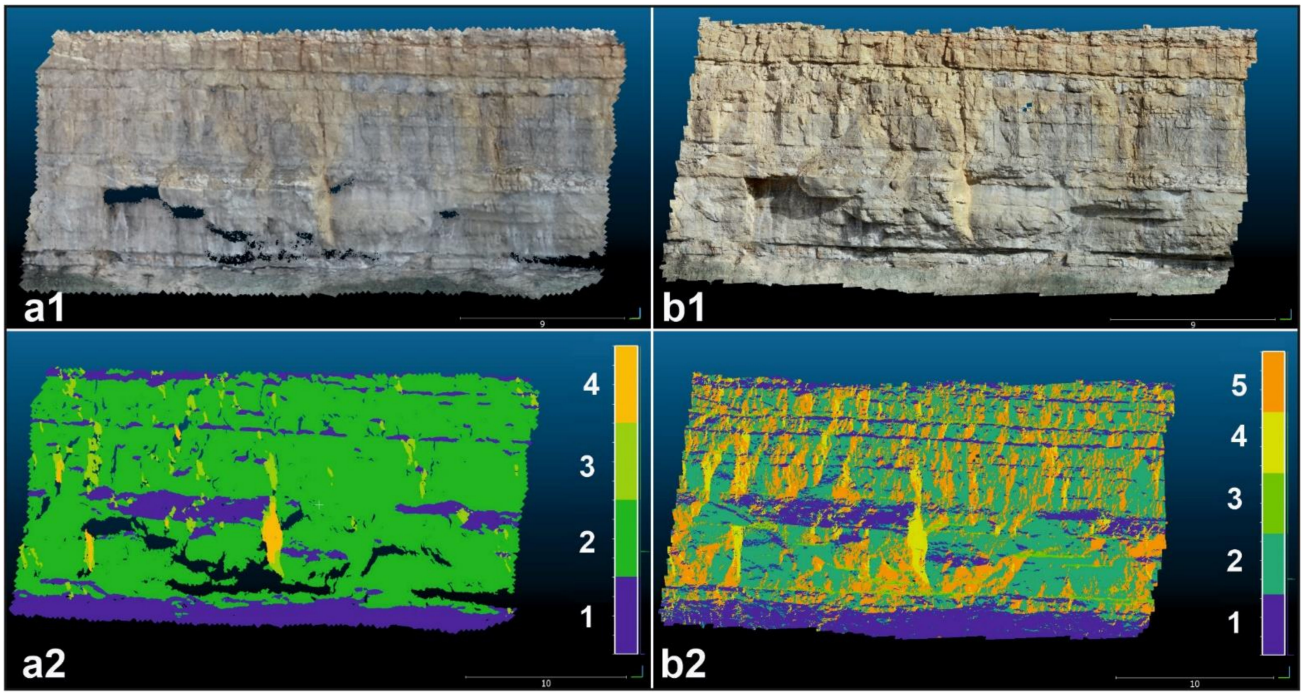

Figure 8. Point clouds (**1**) and discontinuity orientations (**2**) in two drone settings: AMSL-40°-off-nadir (**a**) and facade-nadir (**b**). The number of the legends correspond to the discontinuity orientations of Table 5.

4. Discussion

Mining landscapes usually have high relief complexity, operational constraints, and experience rapid topographic changes. In this context, SfM-UAV surveys offer a reliable, fast, and cheap methodology to monitor these environments, and their use is continuously increasing [26]. However, most of the published results include the detection of changes between two topographies with GSD and accuracies above five centimetres [25]. Topographic surveys with higher GSD and accuracy are needed to study risks and adopt mitigation measurements, to map geologic structures, and to predict rockfalls [6] and slope failures [46], since human lives and the economic viability of an active mine may be endangered. The use of a computer-based program also requires testing on vertical landscapes [16] to save time, improve results, and increase flight safety. We have evaluated alternative drone configurations to conduct SfM-UAV surveys in, relief-wise, the most complex and dangerous zone of a mine: a highwall. These sandstone and rock faces possess challenging conditions to conduct this topographic method: long and vertical surfaces without access to deploy control/check points at the base and crest of highwalls.

4.1. Evaluation of Data Quality: Implications of Flight Altitude Mode and Camera Angle

Our results suggest that the best drone flight setting is a facade drone mode combined with a nadir camera angle (F) in a vertical landscape such as a mining long highwall (Figure 9). This deployment achieved the highest point cloud density and highest accuracy using the lowest field flight and computer processing time. Facade drone mode with 40° off-nadir images (G) also produces a good quality and high-density point cloud. Its void area occurred as the flight was divided in two segments to maintain a constant GSD and inadequate picture overlap was achieved.

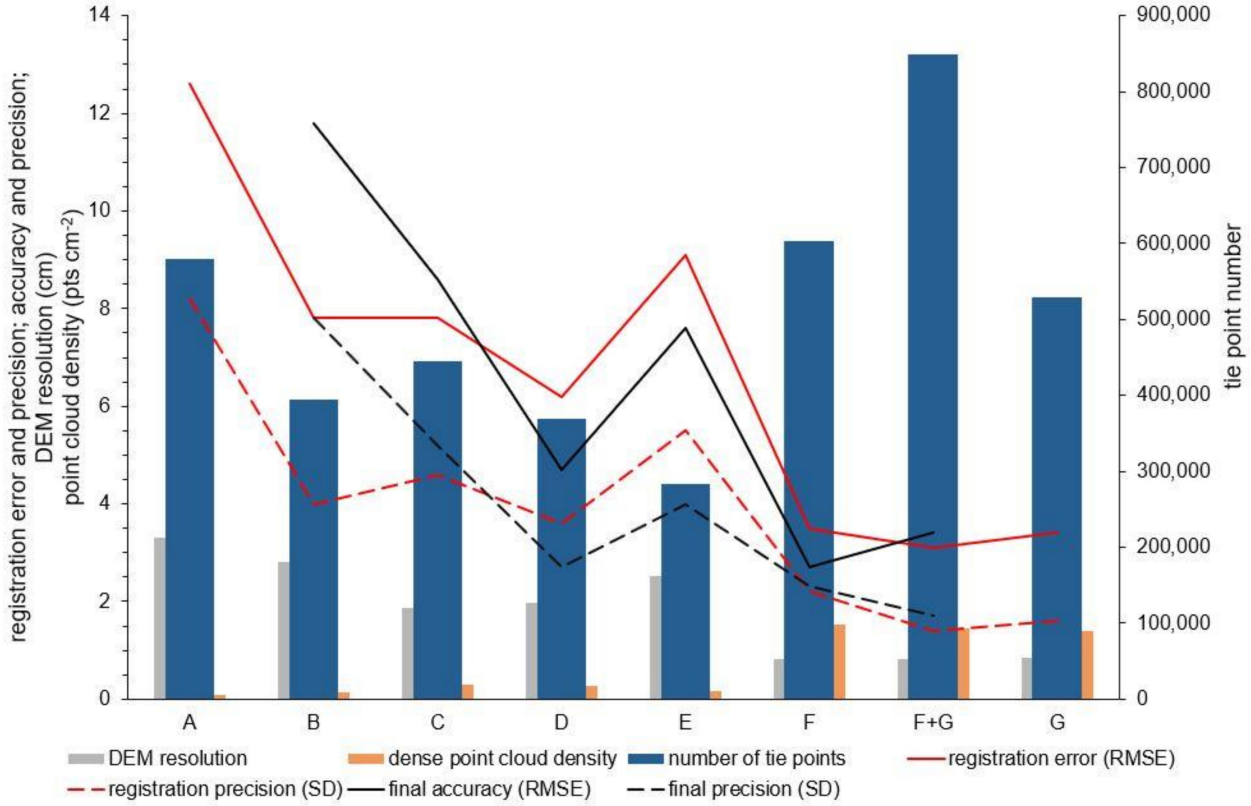

Figure 9. Comparison of the main 3D quality error indicators, (tie and dense) point cloud density and DEM resolution. (**A**) AMSL-nadir; (**B**) AMSL-40° off-nadir; (**C**) AGL-nadir; (**D**) AGL-40° off-nadir, (**E**) AGL-Point of Interest; (**F**) facade-nadir; (**G**) facade-40° off-nadir.

Adding oblique images usually improves SfM survey accuracy in surveys at an AMSL altitude [5] and it is also expected in AGL flight modes. In high-relief landscapes, adding facade images also improves the final accuracy of a UAV-SM procedure [16]; however [16] did not conduct a survey using only facade images with different camera angles (oblique and/or nadir). Our results suggest that in the facade drone mode applied to a quasi-vertical landscape, oblique images do not improve accuracy. Analysis shows that final point cloud density and accuracy may slightly decrease by adding oblique images, although the final precision is better. Adding facade images to AMSL surveys improves the final accuracy in high-relief landscapes [16], however, we did not run this combination because it would negatively affect the topographies obtained in the facade survey, since GSD widely differ. Moreover, facade flight mode ensures a full coverage of the highwall by itself, so AMSL images would not provide additional advantage in regard to the aims of this study.

AMSL surveys (A, B) can produce dense point clouds covering almost all the highwall, but the errors are high and the point density and DEM resolution are low. AGL surveys (C, D) cannot produce a dense point cloud covering the full highwall, having important data voids in the upper section. Although the AGL procedure adapts the drone altitude to the topographic changes, the images can neither fully capture the area nor achieve sufficient overlap, solvable by increasing the overlap in the drone flight mode and the coverage area, but requiring a considerable increase in survey time. Hence this flight altitude mode is unable to assist the capture of feature definitions along large vertical changes in few horizontal meters, as is typical of a highwall surface. Oblique images allow better topographies to be obtained than nadir images in AMSL and AGL modes. The Point of Interest camera angle outcome (E) did not report suitable errors, nor did it reconstruct the full area, therefore the use of this camera angle for the long vertical surface of a highwall was deemed not viable; this option has been demonstrated to be useful in flat areas [20].

The cloud-to-cloud comparisons undertaken with the M3C2 algorithm also showed that only the facade drone survey combined with a nadir camera angle (F) produced a low and almost normal error distribution. For the other drone flight mission settings, significant deviations occurred. We interpret these deviations as being the result of poor control/check point distribution and the limitations of the SfM procedure in reconstructing some areas. The reference TLS point cloud had an accuracy similar to other surveys undertaken in the vicinity [5]. Although some map areas had poor point density or were empty, their points are reliable in terms of position accuracy, since they do not experience the same type of systematic errors experienced by the SfM-UAV survey, such as the doming effect. Hence, it is useful to consider the deviations shown in our investigation when planning future studies.

The most common vertical landscapes monitored with the SfM-UAV procedure are natural cliffs. A ca 5-cm 3D precision and a maximum point density of 0.09 pts cm^{-2} was reported in [19], whereas [47] reported a 3D accuracy of 2.3 cm and a point density of 0.13 pts cm^{-2}, both in coastal areas. In those examples, errors and point densities are similar or worse than those reported in the present study using a facade drone flight mode combined with a nadir camera angle. The main difference in those examples is that the control/check points were deployed at the top and base of the cliffs instead of the common procedure based on distribution over the entire surface [48]. This procedure, validated for coastal cliffs [22], makes sense, since in these cliffs the height varied between 25 and 80 m. However, for longer vertical surveys of highwall faces in mines, points covering the entire survey area are advised to avoid systematic errors as supported by the M3C2 comparisons using TLS as reference. This was also suggested in a recent study carried out in the Isabel II Dam in Spain, where many different control/check point numbers and distributions where evaluated [18].

As for long highwalls, the most detailed study was carried out in a marble quarry in Italy [28], employing a similar procedure as our study. The main difference is that they conducted the vertical drone flights manually, instead of programmed. The 3D accuracy was 3 cm, similar to that obtained in our study (2.4–2.7 cm), however they reported a point density varying from 0.25 to 1 pts cm^{-2}, lower than reported in the facade drone mode and nadir camera angle configuration (F) of this study (1.53 pts cm^{-2}). Manually driving a drone with a vertical trajectory is a difficult task in terms of obtaining a low and constant GSD and with a high overlap, which can prevent generating more detailed point clouds. Overcoming these problems is undertaken by increasing the number of photos, and, consequently, increasing the surveying time. Although conducting vertical flight manually might obtain a highly detailed and accurate topography, the collision risk remains. Our results show how a facade flight mode programmed with a computer-based mission planning software, allows users to conduct SfM-UAV surveys in long highwalls faster, safely and at a higher detail and quality.

4.2. Control/Check Point Survey in Highwalls

Since a drone can be easily programmed with a computer-based mission planning software to follow a facade trajectory and use a nadir camera angle (F), the most difficult task to survey long vertical landscapes with no access is the manner by which to establish control/check points. Being unfeasible to place fixed marks, natural features like rock outcrop edges, joints and faults, and bedding planes need to be used as references. Presently the only available instrument is a robotic total station, which possesses a coaxial camera to allow identification and measurement of points up to 1 km. However, in scenarios without rock and earth fall risk, placing some fixed markers at the bottom of the highwall will improve the evaluation of georeferencing of the final dense point cloud.

While each drone flight lasted 16–29 min, identifying and measuring the reference points throughout the survey area took four hours in this experiment. It was a demanding task, and as the distance to the reference point in the highwall increased, so too did the difficulty. These points should be surveyed considering that it is necessary to later

identify them in the drone photographs during computer processing. Two examples of natural marks in the highwall used as references in the SfM processing are vertices of characteristic shapes: a corner rock and a sand zone with significant color changes (Figure 10). These points were measured at varying distances (90 and 230 m). Figure 10 highlights the importance of how images taken with a drone simplify their identification in an SfM software. A facade drone flight mode combined with a nadir camera angle (F) provides the best images to identify reference points instead of the common AMSL surveys (A, B). This manner of georeferencing SfM-UAV surveys with "natural" points in vertical landscapes was previously suggested [6], however few examples exist. The authors of [49] georeferenced a SfM-UAV survey of a road cut-slope, which had experienced several landslides, following a similar procedure as described herein. The RMSE for each axis varied (5.0–10.1 cm) depending on camera angle and drone flight mode. It was greater than the error obtained for the facade-nadir survey in our study (Table 3). They were unable to measure points over the entire cut-slope due to the selected total station. Others conducted an SfM-UAV survey of a rock outcrop to detect discontinuities following the same method [24]. Their final topography had a precision of 2.3-cm in xy and 0.5-cm in z, very similar to our facade drone mode with nadir pictures, 2.9-cm in xy and 0.2-cm in z. Significant difference exists in point cloud density, since their results yielded 0.1 pts cm^{-2} while our study produced 1.5 pts cm^{-2}. The difference in density and z precision might owe to the manual drone flight instead of our automatic flights to ensure a constant GSD and overlap.

It is well-known that SfM-UAV surveys in high-relief landscapes such as mines need a significant number of control points with a good distribution, a stratified scheme being best [50]. This study also suggests that, although the distance between points (control or check) has a small influence on the final errors, it is advisable to increase the distance between them. Both recommendations may not be achievable in highwalls, since targets cannot be placed and non-contact tools, such as a total station, are required. Our results may have been influenced by the poor number and distribution of control/check points. However, the best drone flight procedure, facade mode with nadir images, was carried out with 17 control and check points, similar to the 21 points used in another long highwall survey [28]. Although additional check points could have improved quality analyses, the TLS point cloud allowed an extra quality evaluation through the comparison of point clouds that show a normal distribution of the error. Both quality evaluation sources, check points and TLS point cloud, yielded a similar final 3D.

This difficulty of identifying control/check points could be overcome if fieldwork is undertaken in two steps. First, a campaign is conducted to seek reflectorless total station point measurements with some drone images taken to test point identification. In a second campaign, all the drone images are surveyed and the SfM procedure can be completed. However, in some areas such as active mines, surveying time needs to be reduced because topographic changes occur rapidly, are remotely located, and risk analysis needs to be undertaken rapidly. In these cases, field work must be limited to a single campaign, as in our study, when total station points and drone images are simultaneously acquired.

The RTK-GNSS UAVs produces high point cloud densities and accurate topographies without control points [51]. Although others have validated this type of survey in low relief landscapes such as rivers [52], this also highlights the need to continue measuring check points to evaluate the quality of the final topographies. These UAVs could overcome the described survey problems of georeferencing highwall surveys. However, they may not be able to service these particular landscapes, since vertical surfaces produce a shadowing effect, preventing RTK GPS from functioning properly [21]. Using an RTK-UAV in mining areas can produce highly accurate topographies in planar coordinates, but with poor results in elevation [53]. If highly accurate topographies are required, control point deployment is required.

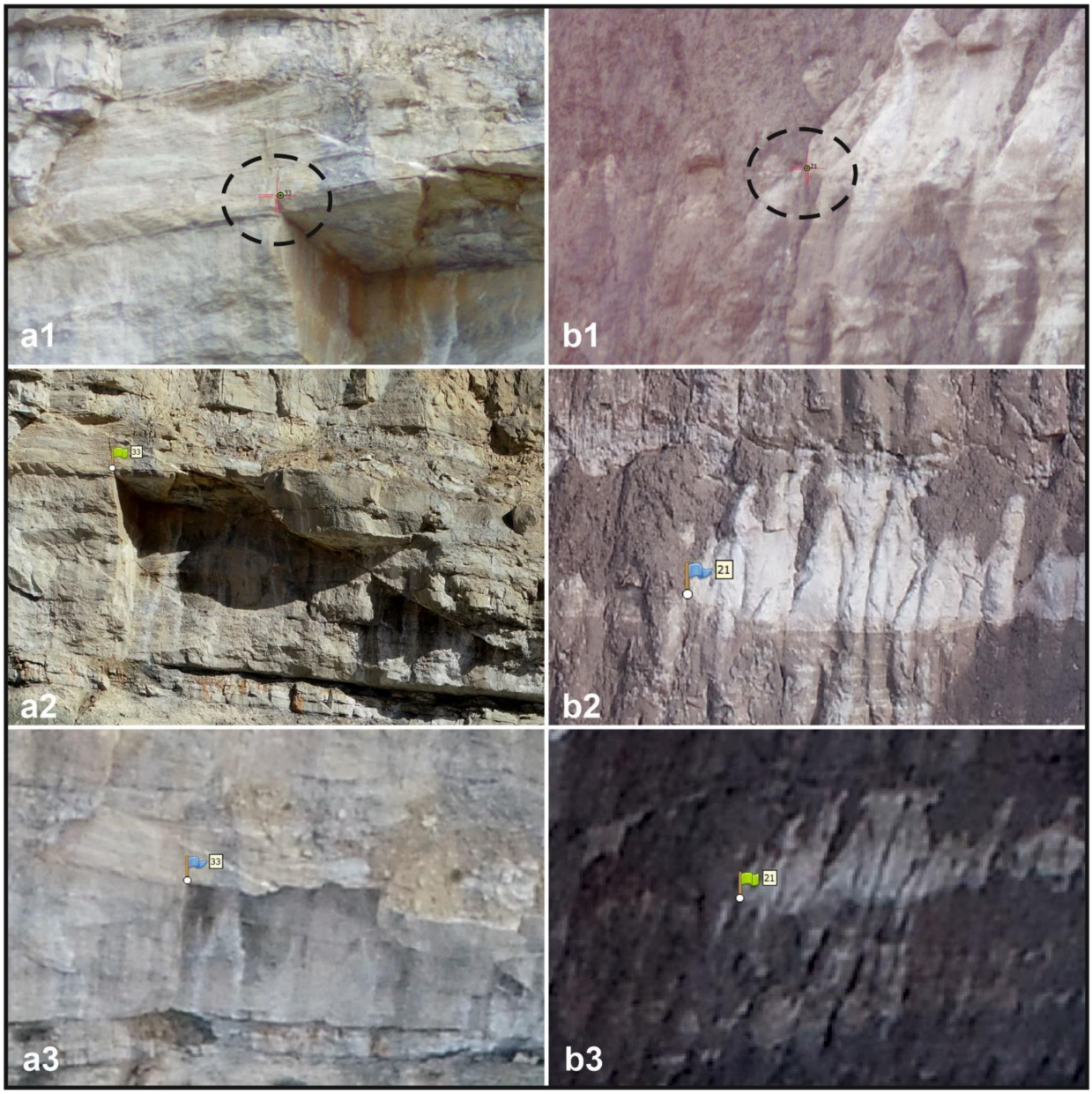

Figure 10. Two types of natural marks measured with the total station (**1**): a characteristic corner edge in a rock (**a**) and a change in color (**b**). These corresponding points are also shown in images taken by the drone in the facade-nadir (**a2**,**b2**) and AMSL-40°-off-nadir (**a3**,**b3**) flights, respectively.

4.3. Use of Detailed Topographies in Monitoring Mining Highwalls

A highwall is critical in active mines and detailed continuous monitoring is required both for operational purposes and to anticipate potential instabilities, mostly by gravitational processes (falls, slides or flows) that can be characterized by topographic discontinuities [54]. High point cloud density and accurate SfM-UAV topographies such as those obtained in this study, with the facade drone flight mode combined with nadir images (F) and georeferenced with a total station, are a reliable method by which to undertake detailed stability analyses. In addition, the survey process is safe, time-saving, economic and contact-free, enabling it to be carried out with high temporal frequency. This can allow the early detection of potential instabilities and risk monitoring of movements.

Methodologies are available to detect joints, areas that can lead to instabilities. A semi-automatic open-source methodology to identify and analyse flat surfaces outcropping

in rocky slopes directly from dense point clouds has been proposed [45]. Its associated software, Discontinuity Set Extraction, was applied to the two topographies that covered almost the full study area with the highest point cloud density and accuracy, AMSL with 40°-off-nadir pictures (B), and facade mode with nadir pictures (F). Again, facade topography offered better results, producing 93.5 % more discontinuities because of its high detail. Indeed, an AMSL topography cannot represent some of the discontinuities because it has insufficient detail, or because it cannot produce points in very intricate areas (Figure 11). The latter was relevant in a few specific zones; discontinuities with potential risk can be present therein.

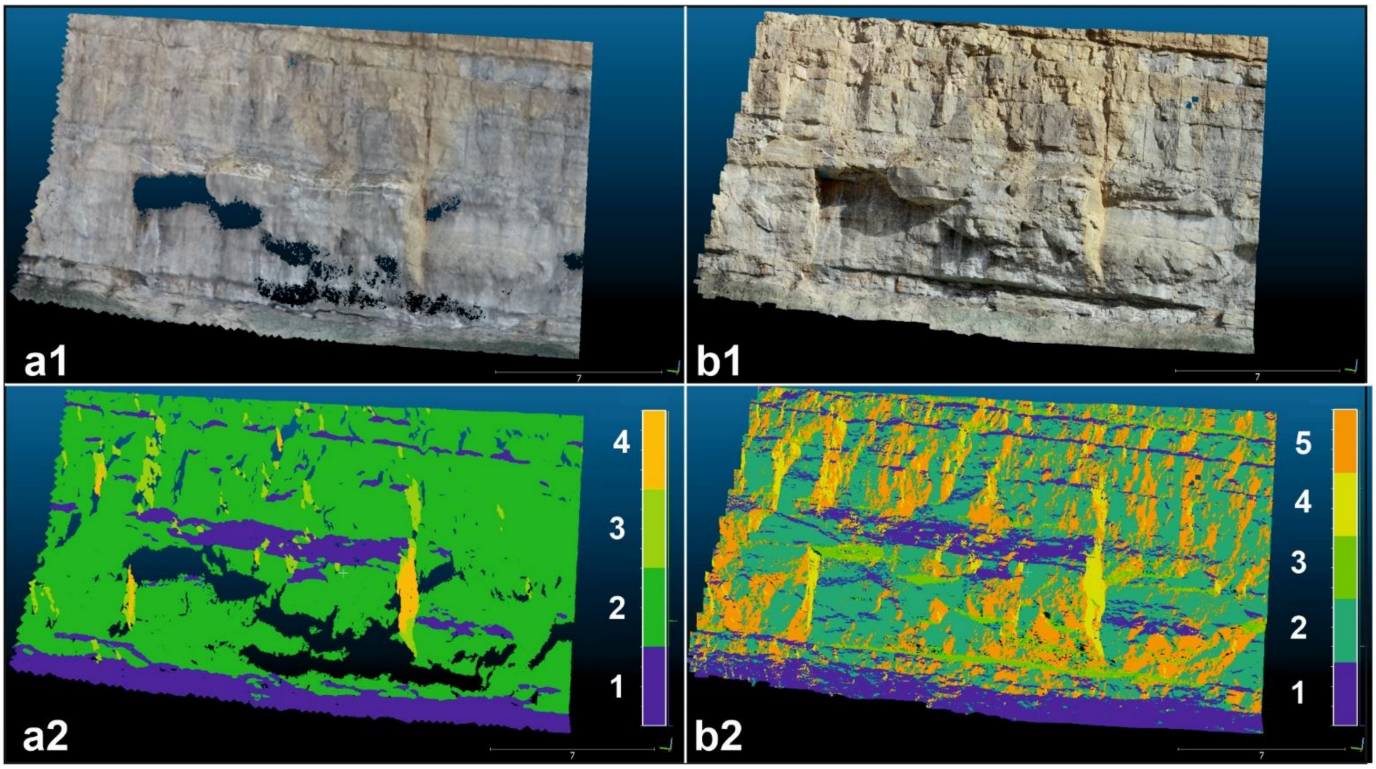

Figure 11. Detail of the point clouds (**1**) and discontinuity clusters (**2**) in two drone settings: AMSL-40°-off-nadir (**a**) and facade-nadir (**b**).

Discontinuities identified by automatic approaches such as those used here need careful validation, since the software can erroneously identify flat features as discontinuities, divide discontinuities in smaller planes, and may fail to detect discontinuities perpendicular to the slope face [55]. This may occur in the set of discontinuities obtained for facade-nadir pictures with Discontinuity Set Extraction software. However, AMSL topographies cannot detect many of them (Figures 8 and 11), supporting the main objective of this study of attaining the best drone setting to obtain topographies of high accuracy and point cloud density for stability analyses. An SfM-UAV survey without control points can be used to identify discontinuities [55]; however, such a topography does not allow precise measurement of displacements between multitemporal surveys. A high correlation between discontinuities detected with the software Discontinuity Set Extraction and those manually mapped can be attained. However, data from the software need to be analysed and validated [44]. Both of these aforementioned studies highlight the ability of this software to quickly recognize a large number of discontinuities. Another algorithm was used by [56] to automatically compare joints and fractures identified though a SfM-UAV topography with those obtained by traditional means, concluding that the automatic procedure detected most of the unfavourable discontinuities existing in the area studied. Detection failures may have occurred because the original point cloud had a density of 0.07

pts cm^{-2} and was georeferenced with few GPS reference points. This can be solved with the workflow proposed in our study. In any case, semi-automatic discontinuity extraction analyses require visual inspection and validation [28]. In this case, we were unable to undertake a field inspection with a compass, because the studied area is inaccessible, rising ca. 100 m above the ground and forming an almost vertical wall.

The discontinuities detected with these topographies may also be used to improve highwall stabilization/reclamation in mine closure plans. Commonly, no adaptative stabilization or sensitive landscape integration measures are applied based on a detailed knowledge of the rock structure. A new approach, the Talus Royal [57], uses a detailed knowledge of rock discontinuities (joints, bedding surfaces or faults) to design final rock outcrops of hard rock surfaces (such as highwalls or roadcuts) that are both stable and blend with the surroundings landscape, by replicating analogue natural cliffs. This method would clearly benefit our methodological contribution.

4.4. Improved SfM-UAV Workflow to Survey Long Highwalls

Many useful SfM-UAV methodologies have been successfully applied to high relief landscapes, but a lack of procedures for near-vertical terrains, such as highwalls, exists [16]. Hitherto only [28] had conducted an SfM-UAV survey in a long highwall to study discontinuity detection. Our results allow improvement to their workflow in terms of saving time, increasing safety and increasing topographic detail and accuracy. Hereafter we detail the steps required to conduct an SfM-UAV survey of a long highwall:

1. measuring control/check points with a robotic total station based on natural shapes;
2. conducting a drone flight programmed with a computer-based mission planning software with the following settings: facade flight mode, double grid with at least 75% forward/side overlap, a nadir camera angle (perpendicular to the highwall), and a constant 40 m highwall distance;
3. processing control/check points and drone images in an SfM software. Since the final aim is to detect discontinuities prone to falls, high detail is required, setting the parameters "accuracy" (alignment step) and "quality" (dense point cloud step), as "Highest" and "Ultra High", respectively. This allows taking advantage of 100% of image quality; and
4. using a semiautomatic discontinuity extraction software and supervising the results with visual inspection of the drone images or the orthophoto obtained after running SfM software.

5. Conclusions

SfM-UAV surveys are entirely incorporated into the workflow of both geomorphology and mine planning projects; however, increased reliability and detail, and a reduction in surveying duration are required. SfM studies in mining areas are usually carried out following traditional workflows based on AMSL drone flight patterns, with the aim to analyse temporal changes throughout an entire area. However, not many studies have conducted specific investigations on highwall faces. These are challenging as they possess some unfavourable features: vertical and long (>100 m) surfaces, no access to the top or base and, if access is available, it is dangerous due to the risk of processes such as rockfalls. A highwall is a key component of the mining industry since minerals are extracted from it. An unexpected disaster may involve human lives and/or fully halt company activity. Frequent high-quality and detailed studies are needed to ensure safe mining production.

We have conducted several drone flights to identify settings that produce the most accurate and detailed topographies in a mining highwall. The results clearly confirm that a facade drone flight mode combined with a nadir camera angle is the best option. Therefore, no extra set of images is needed, as commonly reported in previous publications. This method produces the highest point density, with the highest 3D accuracy, and is efficient in the time required for field work and computer processing. It also allows the detection of more discontinuities than AMSL topographies. Discontinuities from

semiautomatic approaches, as used herein, require careful validation. Such drone settings can be programmed with a computer-based mission planning software, ensuring safe flights and constant and high overlaps and GSDs, without need of an expert pilot. The most problematic, demanding and time-consuming task in the workflow is to identify reference points in the highwall. In this study we used a robotic total station with a coaxial camera that allowed us to complete the surveys, although few points and/or non-well distributed points were measured. Future investigations into highwall SfM surveys should focus on methods to obtain a good georeferentiation. Our findings are an improvement on the current SfM-UAV survey workflows. They can be applied to other mining highwalls or to natural vertical landforms.

Author Contributions: Conceptualization, I.Z.; methodology, I.Z.; data analysis, I.Z.; writing—original draft preparation, I.Z., J.B.L. and J.F.M.D.; writing—review and editing, I.Z., J.B.L., J.F.M.D., L.S.C.; funding acquisition, J.F.M.D., L.S.C. All authors have read and agreed to the published version of the manuscript.

Funding: This study was funded by a postdoctoral grant Torres Quevedo (cofounded by the Spanish Ministry of Science, Innovation and Universities, and Diseño y Desarrollo Minero SL company) conceded to Ignacio Zapico (PTQ-17-09404) and by the Ecological Restoration Network REMEDINAL TE-CM of the Madrid Community (P2018/EMT-4338).

Informed Consent Statement: Not applicable.

Data Availability Statement: The data presented in this study are available on request from the corresponding author. The data are not publicly available due to their size.

Acknowledgments: We thank SPH Engineering for introducing us in their UgCS educational program, A. Herranz (Leica) for support with the MS60 MultiStation, and J.A. Lozano, Á. Moya, J. González, J. de la Villa, R. Peris for their backing. We especially thank David Gutiérrez (DGDRONE), our drone pilot and aerial film maker, Melanie Ball for English editing of the manuscript, Alfonsa Campos, general manager of DDM SL, and Santiago Cano (UCM) for support of statistical data analysis. Three anonymous reviewers made constructive suggestions.

Conflicts of Interest: The authors declare no conflict of interest.

Abbreviations

SfM: Structure from Motion; UAV: Unmanned Aerial Vehicle; TLS: Terrestrial Laser Scanner; GSD: Ground Sampling Distance; AGL: Above Ground Level; AMSL: Above Mean Sea Level; MAE: Mean Absolute Error; RMSE: Root Mean Square Error.

References

1. Mossa, J.; James, L.A. 13.6 Impacts of mining on geomorphic systems. In *Treatise on Geomorphology*; Shroder, J.F., Ed.; Academic Press: San Diego, CA, USA, 2013; pp. 74–95. ISBN 9780080885223.
2. Chen, J.; Li, K.; Chang, K.-J.; Sofia, G.; Tarolli, P. Open-Pit Mining Geomorphic Feature Characterisation. *Int. J. Appl. Earth Obs. Geoinf.* **2015**, *42*, 76–86. [CrossRef]
3. Zapico, I.; Martín Duque, J.F.; Bugosh, N.; Laronne, J.B.; Ortega, A.; Molina, A.; Martín-Moreno, C.; Nicolau, J.M.; Sánchez Castillo, L. Geomorphic Reclamation for Reestablishment of Landform Stability at a Watershed Scale in Mined Sites: The Alto Tajo Natural Park, Spain. *Ecol. Eng.* **2018**, *111*, 100–116. [CrossRef]
4. Carabassa, V.; Montero, P.; Crespo, M.; Padró, J.-C.; Pons, X.; Balagué, J.; Brotons, L.; Alcañiz, J.M. Unmanned Aerial System Protocol for Quarry Restoration and Mineral Extraction Monitoring. *J. Environ. Manag.* **2020**, *270*, 110717. [CrossRef]
5. Zapico, I.; Molina, A.; Laronne, J.B.; Sánchez Castillo, L.; Martín Duque, J.F. Stabilization by Geomorphic Reclamation of a Rotational Landslide in an Abandoned Mine next to the Alto Tajo Natural Park. *Eng. Geol.* **2020**, *264*, 105321. [CrossRef]
6. Giordan, D.; Adams, M.S.; Aicardi, I.; Alicandro, M.; Allasia, P.; Baldo, M.; de Berardinis, P.; Dominici, D.; Godone, D.; Hobbs, P.; et al. The Use of Unmanned Aerial Vehicles (UAVs) for Engineering Geology Applications. *Bull. Eng. Geol. Environ.* **2020**, *79*, 1–45. [CrossRef]
7. Eltner, A.; Sofia, G. Structure from Motion Photogrammetric Technique. *Dev. Earth Surf. Process.* **2020**, *23*, 1–24. [CrossRef]
8. Xu, Q.; Li, W.; Ju, Y.; Dong, X.; Peng, D. Multitemporal UAV-Based Photogrammetry for Landslide Detection and Monitoring in a Large Area: A Case Study in the Heifangtai Terrace in the Loess Plateau of China. *J. Mt. Sci.* **2020**, *17*, 1826–1839. [CrossRef]

9. Özcan, O.; Özcan, O. Multi-Temporal UAV Based Repeat Monitoring of Rivers Sensitive to Flood. *J. Maps* **2020**, *17*, 163–170. [CrossRef]
10. Pineux, N.; Lisein, J.; Swerts, G.; Bielders, C.L.; Lejeune, P.; Colinet, G.; Degré, A. Can DEM Time Series Produced by UAV Be Used to Quantify Diffuse Erosion in an Agricultural Watershed? *Geomorphology* **2017**, *280*, 122–136. [CrossRef]
11. Nesbit, P.; Hugenholtz, C.; Nesbit, P.R.; Hugenholtz, C.H. Enhancing UAV–SfM 3D Model Accuracy in High-Relief Landscapes by Incorporating Oblique Images. *Remote Sens.* **2019**, *11*, 239. [CrossRef]
12. Rodriguez, J.; Macciotta, R.; Hendry, M.T.; Roustaei, M.; Gräpel, C.; Skirrow, R. UAVs for Monitoring, Investigation, and Mitigation Design of a Rock Slope with Multiple Failure Mechanisms—A Case Study. *Landslides* **2020**, *17*, 2027–2040. [CrossRef]
13. Gong, C.; Lei, S.; Bian, Z.; Liu, Y.; Zhang, Z.; Cheng, W.; Gong, C.; Lei, S.; Bian, Z.; Liu, Y.; et al. Analysis of the Development of an Erosion Gully in an Open-Pit Coal Mine Dump during a Winter Freeze-Thaw Cycle by Using Low-Cost UAVs. *Remote Sens.* **2019**, *11*, 1356. [CrossRef]
14. Cucchiaro, S.; Fallu, D.J.; Zhao, P.; Waddington, C.; Cockcroft, D.; Brown, A.G. SfM Photogrammetry for GeoArchaeology. *Dev. Earth Surf. Process.* **2020**, *23*, 183–205. [CrossRef]
15. Kozmus Trajkovski, K.; Grigillo, D.; Petrovič, D. Optimization of UAV Flight Missions in Steep Terrain. *Remote Sens.* **2020**, *12*, 1293. [CrossRef]
16. Tu, Y.-H.; Johansen, K.; Aragon, B.; Stutsel, B.M.; Angel, Y.; Camargo, O.A.L.; Al-Mashharawi, S.K.M.; Jiang, J.; Ziliani, M.G.; McCabe, M.F. Combining Nadir, Oblique, and Façade Imagery Enhances Reconstruction of Rock Formations Using Unmanned Aerial Vehicles. *IEEE Trans. Geosci. Remote Sens.* **2021**, 1–13. [CrossRef]
17. James, M.R.; Robson, S. Mitigating Systematic Error in Topographic Models Derived from UAV and Ground-Based Image Networks. *Earth Surf. Process. Landf.* **2014**, *39*, 1413–1420. [CrossRef]
18. Martínez-Carricondo, P.; Agüera-Vega, F.; Carvajal-Ramírez, F. Use of UAV-Photogrammetry for Quasi-Vertical Wall Surveying. *Remote Sens.* **2020**, *12*, 2221. [CrossRef]
19. Jaud, M.; Letortu, P.; Théry, C.; Grandjean, P.; Costa, S.; Maquaire, O.; Davidson, R.; le Dantec, N. UAV Survey of a Coastal Cliff Face–Selection of the Best Imaging Angle. *Measurement* **2019**, *139*, 10–20. [CrossRef]
20. Sanz-Ablanedo, E.; Chandler, J.H.; Ballesteros-Pérez, P.; Rodríguez-Pérez, J.R. Reducing Systematic Dome Errors in Digital Elevation Models through Better UAV Flight Design. *Earth Surf. Process. Landf.* **2020**, *45*, 2134–2147. [CrossRef]
21. Gilham, J.; Barlow, J.; Moore, R. Detection and Analysis of Mass Wasting Events in Chalk Sea Cliffs Using UAV Photogrammetry. *Eng. Geol.* **2019**, *250*, 101–112. [CrossRef]
22. Westoby, M.J.; Lim, M.; Hogg, M.; Pound, M.J.; Dunlop, L.; Woodward, J. Cost-Effective Erosion Monitoring of Coastal Cliffs. *Coast. Eng.* **2018**, *138*, 152–164. [CrossRef]
23. Ozturk, H.S.; Kocaman, S.; Gokceoglu, C. A Low-Cost Approach for Determination of Discontinuity Orientation Using Smartphone Images and Application to a Part of Ihlara Valley (Central Turkey). *Eng. Geol.* **2019**, *254*, 63–75. [CrossRef]
24. Menegoni, N.; Giordan, D.; Perotti, C.; Tannant, D.D. Detection and Geometric Characterization of Rock Mass Discontinuities Using a 3D High-Resolution Digital Outcrop Model Generated from RPAS Imagery–Ormea Rock Slope, Italy. *Eng. Geol.* **2019**, *252*, 145–163. [CrossRef]
25. Xiang, J.; Chen, J.; Sofia, G.; Tian, Y.; Tarolli, P. Open-Pit Mine Geomorphic Changes Analysis Using Multi-Temporal UAV Survey. *Environ. Earth Sci.* **2018**, *77*, 220. [CrossRef]
26. Braimbridge, M.; Mackenzie, S.; Lyons, M.; Clarke, T.; Bow, B. Whole-of-Landform Erosion Assessment Using Unmanned Aerial Vehicle Data. In Proceedings of the 13th International Conference on Mine Closure, Perth, Australia, 3–5 September 2019; Fourie, A., Tibbett, M., Eds.; Australian Centre for Geomechanics: Perth, Australia, 2019; pp. 397–406.
27. Giacomini, A.; Thoeni, K.; Santise, M.; Diotri, F.; Booth, S.; Fityus, S.; Roncella, R. Temporal-Spatial Frequency Rockfall Data from Open-Pit Highwalls Using a Low-Cost Monitoring System. *Remote Sens.* **2020**, *12*, 2459. [CrossRef]
28. Salvini, R.; Mastrorocco, G.; Esposito, G.; di Bartolo, S.; Coggan, J.; Vanneschi, C. Use of a Remotely Piloted Aircraft System for Hazard Assessment in a Rocky Mining Area (Lucca, Italy). *Nat. Hazards Earth Syst. Sci.* **2018**, *18*, 287–302. [CrossRef]
29. Thoeni, K.; Irschara, A.; Giacomini, A. Efficient Photogrammetric Reconstruction of Highwalls in Open Pit Coal Mines. In Proceedings of the 16th Australasian Remote Sensing and Photogrammetry Conference, Melbourne, Australia, August 2012; pp. 85–90.
30. Ge, L.; Li, X.; Ng, A.H.M. UAV for Mining Applications: A Case Study at an Open-Cut Mine and a Longwall Mine in New South Wales, Australia. In Proceedings of the International Geoscience and Remote Sensing Symposium (IGARSS), Beijing, China, 10–15 July 2016; Institute of Electrical and Electronics Engineers Inc.: Piscataway, NJ, USA, 2016; pp. 5422–5425.
31. Katuruza, M.; Birch, C. The Use of Unmanned Aircraft System Technology for Highwall Mapping at Isibonelo Colliery, South Africa. *J. South Afr. Inst. Min. Metall.* **2019**, *119*, 291–295. [CrossRef]
32. Sayab, M.; Aerden, D.; Paananen, M.; Saarela, P. Virtual Structural Analysis of Jokisivu Open Pit Using 'Structure-from-Motion' Unmanned Aerial Vehicles (UAV) Photogrammetry: Implications for Structurally-Controlled Gold Deposits in Southwest Finland. *Remote Sens.* **2018**, *10*, 1296. [CrossRef]
33. Kong, D.; Saroglou, C.; Wu, F.; Sha, P.; Li, B. Development and Application of UAV-SfM Photogrammetry for Quantitative Characterization of Rock Mass Discontinuities. *Int. J. Rock Mech. Min. Sci.* **2021**, *141*, 104729. [CrossRef]
34. Martín-Moreno, C.; Martín Duque, J.F.; Nicolau Ibarra, J.M.; Muñoz-Martín, A.; Zapico, I. Waste Dump Erosional Landform Stability—A Critical Issue for Mountain Mining. *Earth Surf. Process. Landf.* **2018**, *43*, 1431–1450. [CrossRef]

35. Zapico, I.; Laronne, J.B.; Meixide, C.; Sánchez Castillo, L.; Martín Duque, J.F. Evaluation of Sedimentation Pond Performance for a Cleaner Water Production from an Open Pit Mine at the Edge of the Alto Tajo Natural Park. *J. Clean. Prod.* **2021**, *280*, 124408. [CrossRef]
36. Zapico, I.; Laronne, J.B.; Martín-Moreno, C.; Martín-Duque, J.F.; Ortega, A.; Sánchez-Castillo, L. Baseline to Evaluate Off-site Suspended Sediment-related Mining Effects in the Alto Tajo Natural Park, Spain. *Land Degrad. Dev.* **2017**, *28*, 232–242. [CrossRef]
37. SPH Engineering Ground Station Software | UgCS PC Mission Planning. 2020. Available online: https://www.ugcs.com/photogrammetry-tool-for-land-surveying (accessed on 15 January 2020).
38. Agisoft Agisoft Metashape. 2020. Available online: https://www.agisoft.com/downloads/installer/ (accessed on 15 January 2020).
39. Agüera-Vega, F.; Carvajal-Ramírez, F.; Martínez-Carricondo, P. Assessment of Photogrammetric Mapping Accuracy Based on Variation Ground Control Points Number Using Unmanned Aerial Vehicle. *Measurement* **2017**, *98*, 221–227. [CrossRef]
40. USGS Unmanned Aircraft Systems Data Post-Processing Structure-from-Motion Photogrammetry. 2017. Available online: https://uas.usgs.gov/nupo/pdf/PhotoScanProcessingDSLRMar2017.pdf (accessed on 1 July 2019).
41. James, M.R.; Chandler, J.H.; Eltner, A.; Fraser, C.; Miller, P.E.; Mills, J.P.; Noble, T.; Robson, S.; Lane, S.N. Guidelines on the Use of Structure-from-motion Photogrammetry in Geomorphic Research. *Earth Surf. Process. Landf.* **2019**, *44*, 2081–2084. [CrossRef]
42. CloudCompare. Cloud Compare Version 2.6.1. 2015. Available online: https://www.danielgm.net/cc/ (accessed on 8 January 2020).
43. Lague, D.; Brodu, N.; Leroux, J. Accurate 3D Comparison of Complex Topography with Terrestrial Laser Scanner: Application to the Rangitikei Canyon (N-Z). *ISPRS J. Photogramm. Remote Sens.* **2013**, *82*, 10–26. [CrossRef]
44. Villarreal, J.C.A.; Rojas, D.J.D.; Ríos, R.C.A. 3D Digital Outcrop Modelling of the Lower Cretaceous Los Santos Formation Sandstones, Mesa de Los Santos Region (Colombia): Implications for Structural Analysis. *J. Struct. Geol.* **2020**, *141*, 104214. [CrossRef]
45. Riquelme, A.J.; Abellán, A.; Tomás, R.; Jaboyedoff, M. A New Approach for Semi-Automatic Rock Mass Joints Recognition from 3D Point Clouds. *Comput. Geosci.* **2014**, *68*, 38–52. [CrossRef]
46. López-Vinielles, J.; Ezquerro, P.; Fernández-Merodo, J.A.; Béjar-Pizarro, M.; Monserrat, O.; Barra, A.; Blanco, P.; García-Robles, J.; Filatov, A.; García-Davalillo, J.C.; et al. Remote Analysis of an Open-Pit Slope Failure: Las Cruces Case Study, Spain. *Landslides* **2020**, *17*, 2173–2188. [CrossRef]
47. Gómez-Gutiérrez, Á.; Rito Gonçalves, G. Surveying Coastal Cliffs Using Two UAV Platforms (Multi-Rotor and Fixedwing) and Three Different Approaches for the Estimation of Volumetric Changes. *Int. J. Remote Sens.* **2020**, *41*, 8143–8175. [CrossRef]
48. Sanz-Ablanedo, E.; Chandler, J.; Rodríguez-Pérez, J.; Ordóñez, C. Accuracy of Unmanned Aerial Vehicle (UAV) and SfM Photogrammetry Survey as a Function of the Number and Location of Ground Control Points Used. *Remote Sens.* **2018**, *10*, 1606. [CrossRef]
49. Agüera-Vega, F.; Carvajal-Ramírez, F.; Martínez-Carricondo, P.; Sánchez-Hermosilla López, J.; Mesas-Carrascosa, F.J.; García-Ferrer, A.; Pérez-Porras, F.J. Reconstruction of Extreme Topography from UAV Structure from Motion Photogrammetry. *Measurement* **2018**, *121*, 127–138. [CrossRef]
50. Cabo, C.; Sanz-Ablanedo, E.; Roca-Pardinas, J.; Ordonez, C. Influence of the Number and Spatial Distribution of Ground Control Points in the Accuracy of UAV-SfM DEMs: An Approach Based on Generalized Additive Models. *IEEE Trans. Geosci. Remote Sens.* **2021**, 1–10. [CrossRef]
51. Turner, D.; Lucieer, A.; Wallace, L. Direct Georeferencing of Ultrahigh-Resolution UAV Imagery. *IEEE Trans. Geosci. Remote Sens.* **2014**, *52*, 2738–2745. [CrossRef]
52. Stott, E.; Williams, R.D.; Hoey, T.B. Ground Control Point Distribution for Accurate Kilometre-Scale Topographic Mapping Using an RTK-GNSS Unmanned Aerial Vehicle and SfM Photogrammetry. *Drones* **2020**, *4*, 55. [CrossRef]
53. Hugenholtz, C.; Brown, O.; Walker, J.; Barchyn, T.; Nesbit, P.; Kucharczyk, M.; Myshak, S. Spatial Accuracy of UAV-Derived Orthoimagery and Topography: Comparing Photogrammetric Models Processed with Direct Geo-Referencing and Ground Control Points. *Geomatica* **2016**, *70*, 21–30. [CrossRef]
54. Manzoor, S.; Liaghat, S.; Gustafson, A.; Johansson, D.; Schunnesson, H. Establishing Relationships between Structural Data from Close-Range Terrestrial Digital Photogrammetry and Measurement While Drilling Data. *Eng. Geol.* **2020**, *267*, 105480. [CrossRef]
55. Menegoni, N.; Giordan, D.; Perotti, C. Reliability and Uncertainties of the Analysis of an Unstable Rock Slope Performed on RPAS Digital Outcrop Models: The Case of the Gallivaggio Landslide (Western Alps, Italy). *Remote Sens.* **2020**, *12*, 1635. [CrossRef]
56. Fazio, N.L.; Perrotti, M.; Andriani, G.F.; Mancini, F.; Rossi, P.; Castagnetti, C.; Lollino, P. A New Methodological Approach to Assess the Stability of Discontinuous Rocky Cliffs Using In-Situ Surveys Supported by UAV-Based Techniques and 3-D Finite Element Model: A Case Study. *Eng. Geol.* **2019**, *260*, 105205. [CrossRef]
57. Génie Géologique the Talus Royal Method Website. Available online: http://www.2g.fr/ (accessed on 22 February 2020).